

Structure Preserving Stain Normalization of Histopathology Images Using Self-Supervised Semantic Guidance

Dwarikanath Mahapatra¹, Behzad Bozorgtabar^{2,3,4}, Jean-Philippe Thiran^{2,3,4},
and Ling Shao^{1,5}

¹ Inception Institute of Artificial Intelligence, Abu Dhabi, UAE
{dwarikanath.mahapatra, ling.shao}@inceptioniai.org

² Signal Processing Laboratory 5, EPFL, Lausanne, Switzerland
{behzad.bozorgtabar, jean-philippe.thiran}@epfl.ch

³ Department of Radiology, Lausanne University Hospital, Lausanne, Switzerland

⁴ Center of Biomedical Imaging, Lausanne, Switzerland

⁵ Mohamed bin Zayed University of Artificial Intelligence, Abu Dhabi, UAE

Abstract. Although generative adversarial network (GAN) based style transfer is state of the art in histopathology color-stain normalization, they do not explicitly integrate structural information of tissues. We propose a self-supervised approach to incorporate semantic guidance into a GAN based stain normalization framework and preserve detailed structural information. Our method does not require manual segmentation maps which is a significant advantage over existing methods. We integrate semantic information at different layers between a pre-trained semantic network and the stain color normalization network. The proposed scheme outperforms other color normalization methods leading to better classification and segmentation performance.

Keywords: GANs · Semantic guidance · Color normalization · Digital pathology.

1 Introduction

Increased digitization of pathology slides has enhanced the importance of digital histopathology in the medical imaging community [15,81,23,12,10,58,51]. Staining is an important part of pathological tissue preparation where, e.g., Hematoxylin and Eosin dyes alter the intensity of tissue elements - nuclei turn dark purple while other structures become pink. Tissue structures become distinguishable, facilitating manual or automated analysis.

The color variation of the same structure is observed due to differences in staining protocols from different centers, different dye manufacturers, and scanner characteristics. Consequently, this leads to inconsistent diagnosis and limits the efficacy of automated methods. Hence there is a need for stain color normalization to have a uniform appearance of dye-stained regions. We propose

to integrate self-supervised semantic guidance with GANs for better structure preservation after stain normalization.

Two widely explored categories for stain normalization methods are color matching [119,147,114,66,49,36,48,84], and stain-separation [38,30,68,69,85,88,45,44,47]. Since these methods rely on template images, it leads to mismatch and poor performance when the template is not representative of the dataset. The third category comprises machine learning approaches [28,43,108,106,104,60,32,13] which sub-divide an input image into multiple tissue regions using a sparse auto-encoder, and independently normalize each region. Recent works solve stain normalization as a style-transfer problem using Generative adversarial networks (GANs) [9,140,80,63,83,127,128,55]. GANs have found many applications in medical image analysis [141,29,129,62,123,122,136,131,92] such as image super-resolution [59,117,116,118], registration [81,130,91,146,65,64,70,89], segmentation [143,63,113,34,87,126,86,96,125], domain adaptation [18,14,16,17,46,67,112,110,111,109,40,42] and data augmentation [60,10,138,41,39,107,101,102,103,105] to name a few. Unpaired Image-to-Image Translation with CycleGANs were used in [132,98,99,95,93,100,115,90,53,61] to facilitate style transfer across two domains. These methods do not require a reference image and achieve high visual agreement with images from the target domain. Gupta et al. [26,124,11,52,79,57,33,24,97,56] leverage GAN based image-image translation for data augmentation of histopathology images, yielding an improvement in segmentation accuracy. Other variants include the use of prior latent variables and auxiliary networks [142,50,54,7,71,72,76,6,75,5], and auxiliary inputs [144].

Previous works have demonstrated the effectiveness of cycle GANs in stain normalization, thus eliminating the tedious task of selecting a reference stain. However, as pointed out in [21,77,78,74,73,94,82,22,3] shape outlines of translated objects may change which leads to sub-optimal performance. Gadermayr [21] used two different pipelines to overcome this pitfall. While their results are effective, the pipeline itself is tedious. Vahadane et al. [137] propose a structure-preserving normalization method using non-negative matrix factorization but do not explicitly use semantic information. Lahiani et al. [35] introduce a perceptual embedding loss to reducing tiling artifacts in reconstructed whole slide images (WSI).

Self-supervised learning requires formulating a proxy (or pretext) task, which can be solved on the same dataset and using the trained network to perform self-supervised tasks such as segmentation or depth estimation [25]. Some examples in the field of medical image analysis include divide-and-rule framework for survival analysis in colorectal cancer [2], surgical video re-colorization as a pretext task for surgical instrument segmentation [121], rotation prediction for lung lobe segmentation and nodule detection [135] and use disease bounding box localization for cardiac MR image segmentation [4].

Contributions: Since medical image analysis influences diagnostic decisions, it is helpful to preserve information about more delicate structures for semantic guidance. The inclusion of segmentation information requires detailed anno-

tations of the image, which is extremely cumbersome for WSIs. Our primary contribution is a color stain normalization method that uses semantic guidance through self-supervised features. We build our model using cyclic GANs [145,81] as they are an effective choice for transferring image appearances across domains. Semantic guidance is incorporated using a pre-trained semantic segmentation network trained on a different dataset. Semantic information in the form of segmentation feature maps from multiple levels is injected into the stain normalization network. Since we use self-supervised segmentation maps, we do not need manual annotations during training or test stages, which makes it easy to deploy for novel test cases. Our paper makes the following contributions:

- we integrate self-supervised features for stain normalization using semantic guidance from a pre-trained network;
- self-supervised segmentation feature maps allow us to use our method despite the unavailability of manual segmentation maps. Our proposed method beats the state-of-the-art stain normalization methods when the normalized images are used for classification and segmentation tasks.
- Different from [35], we explicitly use semantic information to capture geometric and structural patterns for image normalization. In particular, we use pixel adaptive convolution to match fine-grained segmentation maps of normalized images.

2 Method

We denote the set of training images as I_{Tr} , their labels (manual segmentation masks or disease class) as L_{Tr} , and the trained model (segmentation or classification) as M_{Tr} . Given a set of test images I_{Test} , our objective is to segment/classify them using the pre-trained model M_{Tr} . To successfully do that, we: 1) color normalize the test images using our proposed method SegCN-Net; and 2) apply pre-trained M_{Tr} .

Figure 1 depicts the workflow of our proposed stain normalization method. There are three different networks, G_{AB} (the generator network in red), Seg_{Sem} (the pre-trained segmentation network in yellow providing semantic guidance), and G_{BA} (the generator network in green). All three networks are based on a UNet architecture [120] to facilitate the easy integration of semantic information during training and test phases. G_{AB} transforms A to look like an image from domain B while G_{BA} performs the reverse translation to maintain cycle consistency. Images from A and B are passed through Seg_{Sem} and the information from different layers of Seg_{Sem} is fused with the corresponding layer of G_{AB} and G_{BA} to facilitate the integration of semantic guidance.

2.1 Semantic Guidance Through Self-Supervised Learning

Our self-supervised approach does not define any pretext task but focuses on using pre-trained networks for semantic guidance in stain normalization. Semantic

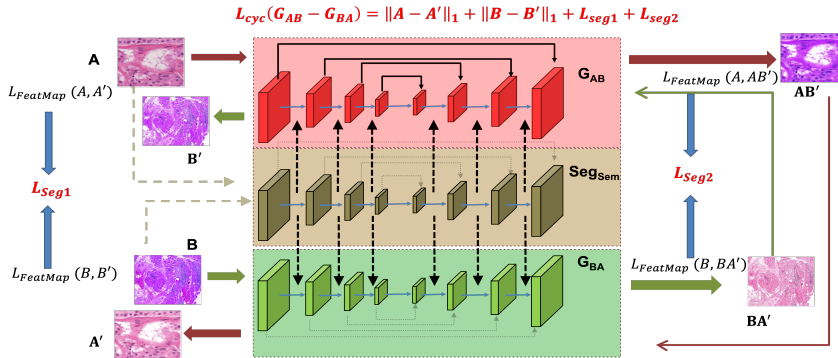


Fig. 1. The workflow of our proposed stain color normalization method using CycleGANs. Semantic guidance is injected from the corresponding layers of Seg_{Sem} into the generators G_{AB} , G_{BA} , and helps to preserve critical cellular structures in normalization.

features for guiding the stain normalization task come from the pre-trained segmentation network Seg_{Sem} shown in Figure 1. Seg_{Sem} 's pre-trained weights guide the feature learning process of the two generators without the need for further finetuning.

The translation invariance property of standard convolution makes it content-agnostic. It poses certain limitations, such as despite reducing the number of parameters, it may lead to sub-optimal learning of feature representations. Additionally, spatially-shared filters globally average loss gradients over the entire image, and the learned weights can only encode location-specific information within their limited receptive fields. Content-agnostic filters find it difficult to distinguish between visually similar pixels of different regions (e.g., dark areas due to artifacts or tissues) or learn to identify similar objects of different appearances (e.g., same tissue structure with different shades as in our problem).

Pixel-adaptive convolutions [134] can address the above limitations where the feature representations encoded in the semantic network help distinguish between confounding regions, and are defined as:

$$\mathbf{v}'_i = \sum_{j \in \Omega(i)} K(\mathbf{f}_i, \mathbf{f}_j) \mathbf{W} [\mathbf{p}_i - \mathbf{p}_j] \mathbf{v}_j + b \quad (1)$$

where \mathbf{f} are the features from the semantic network that guide the pixel adaptive convolutions, \mathbf{p} are pixel co-ordinates, \mathbf{W} is the convolutional weights of kernel size k , Ω_i is a $k \times k$ convolution window around pixel i , \mathbf{v} is the input and b is the bias term. For each feature map, we apply a 3×3 and a 1×1 convolution layer followed by Group Normalization [139] and exponential linear units (ELU) non-linearities [20]. The resulting semantic feature maps are fused with the corresponding layers of G_{AB} and G_{BA} and used as guidance on their respective

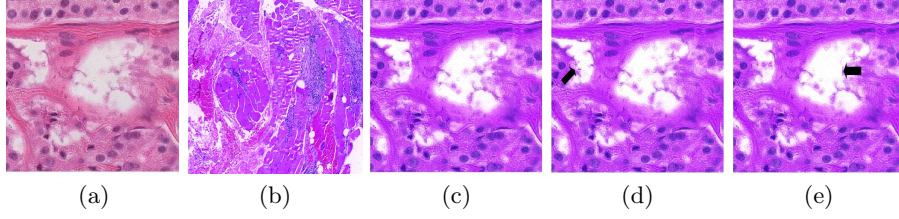


Fig. 2. Color normalization results: (a) Domain A image; (b) Domain B image; Domain A transformed to Domain B using: (c) proposed *SegCN-Net*; (d) [21]; (e) [144]. Areas of structure inconsistency are shown by black arrows.

pixel-adaptive convolutional layers. K is a standard Gaussian kernel defined by:

$$K(\mathbf{f}_i, \mathbf{f}_j) = \exp\left(-\frac{1}{2}(\mathbf{f}_i - \mathbf{f}_j)^T \Sigma_{ij}^{-1}(\mathbf{f}_i - \mathbf{f}_j)\right) \quad (2)$$

where Σ_{ij}^{-1} is the covariance matrix between feature vectors $\mathbf{f}_i, \mathbf{f}_j$ and formulated as a diagonal matrix $\sigma^2 \cdot I_D$, where σ is an additional learnable parameter for each filter. Standard convolution is a special case when $K(\mathbf{f}_i, \mathbf{f}_j) = 1$.

To capture semantic information across multiple scales, we extract the feature maps after each convolution stage to get a set of maps with varying dimensions due to max pooling operations, whose values are normalized to $[0, 1]$. For a given pair of images, we calculate the mean squared error between f_s - corresponding multi-scale feature maps. Thus, the feature map loss between a and \hat{a} is:

$$L_{FeatMap}(a, \hat{a}) = \sum_{s=1}^S \sqrt{\frac{(f_s(a) - f_s(\hat{a}))^2}{N}} \quad (3)$$

2.2 Color Normalization Using Semantic Guidance

Cycle GANs transform an image from domain A to B , and the reverse translation from B to A should generate the original input image. In forward cycle consistency, an image from domain A is translated to domain B by generator G_{AB} expressed as $\hat{b} = G_{AB}(a)$. Image \hat{b} is translated back to domain A by G_{BA} to get $\hat{a} = G_{BA}(\hat{b})$. Similarly, the original and reconstructed images from B should also match. Thus the overall cycle consistency loss is:

$$L_{cycle}(G_{AB}, G_{BA}) = E_a \|a - G_{BA}(G_{AB}(a))\|_1 + \|b - G_{AB}(G_{BA}(b))\|_1 + L_{Seg}, \quad (4)$$

$$L_{Seg} = \underbrace{L_{FeatMap}(a, \hat{a}) + L_{FeatMap}(b, \hat{b})}_{L_{Seg1}} + \underbrace{L_{FeatMap}(a, \hat{a}\hat{b}) + L_{FeatMap}(b, \hat{b}\hat{a})}_{L_{Seg2}} \quad (5)$$

We impose the additional constraint that the fine-grained segmentation maps of images should match, not just of the reverse transformed images a, \hat{a} and b, \hat{b}

but also between the outputs of each generator and the corresponding original images, i.e. between a, \hat{a} and \hat{b}, b . L_{Seg2} is specifically designed to preserve structural information between images of domain A, B in stain normalization.

Discriminator D_B is employed to distinguish between real image b and generated image \hat{a} where the adversarial loss in forward cycle, L_{adv} , is:

$$L_{adv}(G_{AB}, D_B, A, B) = E_b \log D_B(b) + E_a \log [(1 - D_B(G_{AB}(a)))]. \quad (6)$$

There also exists a corresponding $L_{adv}(G_{BA}, D_A, B, A)$ to distinguish between real image a and generated image \hat{b} . Thus the final objective function is:

$$L = L_{adv}(G_{AB}, D_B, A, B) + L_{adv}(G_{BA}, D_A, B, A) + L_{cyc}(G_{AB}, G_{BA}) \quad (7)$$

Network Architecture All the networks ($G_{AB}, G_{BA}, Seg_{Sem}$) are based on a UNet architecture [120] with a ResNet backbone. Each convolution block has 3 layers of convolution layers (all using the adaptive pixel convolutions and ELU), followed by a 2×2 max-pooling step of stride 2. Skip connections exist between the stages of the contracting and expanding path. 3×3 kernels are used with adequate padding to maintain image dimensions. There are four convolution blocks in both paths.

3 Experimental Results

3.1 Evaluation Set Up for Classification

Our proposed color normalization method is SegCN-Net (segmentation based color normalization network), and evaluate its performance as a pre-processing step. CAMELYON16 [8] and CAMELYON17 [19] public datasets are used to have WSIs for classification and segmentation of breast cancer metastases. CAMELYON16 has images from 2 independent medical centers, while CAMELYON17’s images come from 5 centers. We train SegCN-Net on CAMELYON16 and evaluate on transformed images of CAMELYON17. Domain A consists of images from Center 1 of CAMELYON16 ($C_{1_{16}}$), while domain B has images from $C_{2_{16}}$. 100,000 patches of 256×256 were extracted from each domain, and we train all models using an NVIDIA Titan X GPU having 12 GB RAM, Adam optimizer [31] with a learning rate of 0.002. Xavier initialization was used, and training took 42 hours for 150 epochs with batch size 16.

For evaluation, images from the different centers of CAMELYON17 were split into training/validation/test in 50/30/20% to obtain the following split: $C_{1_{17}}$:37/22/15, $C_{2_{17}}$: 34/20/14, $C_{3_{17}}$: 43/24/18, $C_{4_{17}}$: 35/20/15, $C_{5_{17}}$: 36/20/15. For our first baseline, we train 5 different ResNet50 [27] with batch size 32, Adam optimizer learning rate of 0.001 for 70 epochs (denoted as **ResNet**_{NoNorm}) on images from $C_{1_{17}} - C_{5_{17}}$ using the split described before, but without normalization. We apply SegCN-Net on images from different centers of CAMELYON17 to color normalize them and train ResNet50 networks with similar settings as *ResNet*_{NoNorm} using the data split of $C_{1_{17}} - C_{2_{17}}$. The results (using the area

Table 1. Classification results in terms of AUC measures for different stain normalization methods on the CAMELYON17 dataset. p values are with respect to SegCN-Net.

Method	<i>Center 1</i>	<i>Center 2</i>	<i>Center 3</i>	<i>Center 4</i>	<i>Center 5</i>	<i>Average</i>	p
<i>ResNet_{C17noNorm}</i>	0.8068	0.7203	0.7027	0.8289	0.8203	0.7758	0.0001
Reinhard [119]	0.7724	0.7934	0.8041	0.8013	0.7862	0.7915	0.0001
Macenko [38]	0.7148	0.7405	0.8331	0.7412	0.7436	0.7546	0.0001
CycleGAN	0.9010	0.7173	0.8914	0.8811	0.8102	0.8402	0.002
Vahadane [137]	0.9123	0.7347	0.9063	0.8949	0.8223	0.8541	0.003
Zhou [144]	0.9381	0.7614	0.7932	0.9013	0.9227	0.8633	0.013
Gadermayr [21]	0.9487	0.8115	0.8727	0.9235	0.9351	0.8983	0.013
SegCN-Net	0.9668	0.8537	0.9385	0.9548	0.9462	0.9320	-
Ablation Study Results							
SegCN-Net _{Conv}	0.9331	0.8255	0.9148	0.9259	0.9181	.9035	0.0008
SegCN-Net _{Seg Only}	0.9376	0.7974	0.8942	0.9187	0.9012	0.8898	0.0001
SegCN-Net _{C17Rand}	0.9624	0.8403	0.9267	0.9478	0.9391	0.9232	0.34
SegCN-Net _{Glas}	0.9762	0.8627	0.9509	0.9677	0.9588	0.9432	0.042

under the curve (AUC) as the performance metric) are reported in Table 1 under SegCN-Net. We replace our stain normalization method with other competing methods, such as [144,119,38,137,21] and perform the same set of classification experiments with the performance summarized in Table 1.

[137] aims to preserve structure information through templates while [144] employ stain color matrix matching. Since they do not explicitly use segmentation information, SegCN-Net performs better than both methods. The method by [21] does better than others because of the use of segmentation information but requires labeled segmentation maps. SegCN-Net’s superior performance shows that the use of self-supervised segmentation can be leveraged when manual segmentation maps are not available. Figure 2 shows the stain normalized images of different methods. The advantage of SegCN-Net in preserving structural information is indicated by the black arrows where the glandular structure is deformed from the original image in [144], and to a lesser extent in [21]. Thus the advantages of our semantic guidance based stain normalization are obvious.

3.2 Ablation Studies

Table 1 summarizes the performance of the following variants of our method:

1. SegCN-Net_{Conv} - *SegCN-Net* using standard convolutions instead of pixel adaptive convolutions.
2. SegCN-Net_{Seg} - SegCN-Net using only the final segmentation masks without the intermediate feature map. This evaluates the relevance of using a single segmentation map without semantic guidance at each layer.
3. SegCN-Net_{C17Rand} - SegCN-Net tested on all normalized images of C17 with a random selection of train/val/split. The results are an average of 10 runs and investigate possible bias in data split.

In the original approach, Seg_{Sem} was pre-trained on the MS-COCO dataset [37]. In a variant of our proposed method, we use a network pre-trained on the Glas segmentation challenge dataset [133], which has segmentation masks of histological images and use it for classification of the test images from CAMELYON17. The results are shown in Table 1 under SegCN-Net $_{Glas}$.

SegCN-Net $_{Glas}$ shows better classification performance than SegCN-Net and the difference in results at $p = 0.042$ is significant as semantic guidance is obtained from a network trained on histology images, while SegCN-Net used natural images. Although natural images provide some degree of semantic guidance by learning edge features, Seg_{Sem} trained on histopathology images provides domain-specific guidance and hence leads to better performance. Since such an annotated dataset is not always available for medical images, we show that semantic guidance from a network trained on natural images significantly improves the state-of-art method for stain color normalization.

SegCN-Net $_{C17Rand}$ performance is close to SegCN-Net without any statistically significant the difference, indicating that SegCN-Net is not biased on the test set. SegCN-Net $_{Seg Only}$ shows inferior performance compared to SegCN-Net, which indicates that multistage semantic guidance is much better than a single segmentation map. However SegCN-Net $_{Seg Only}$ still performs slightly better than [21] indicating the advantages of including segmentation information for structure-preserving color normalization.

3.3 Segmentation Results

We apply our method on the public GLAS segmentation challenge [133], which has manual segmentation maps of glands in 165 $H\&E$ stained images derived from 16 histological sections from different patients with stage $T3$ or $T4$ colorectal adenocarcinoma. We normalize the images using SegCN-Net (using MS-COCO images for semantic guidance), train a UNet with residual convolution blocks, and apply on the test set. The performance metrics - Dice Metric (DM), Hausdorff distance (HD), F1 score (F1)- for SegCN-Net, [144,21] and the top-ranked method [1] are summarized in Table 2. [144]’s performance comes close to the top-ranked while [21] outperforms both of them, and SegCN-Net gives the best results across all three metrics. This shows that stain normalization, in general, does a good job of standardizing image appearance, which in turn improves segmentation results. SegCN-Net performs best due to the integration of segmentation information through self-supervised semantic guidance.

3.4 Color Constancy Results

Similar to [142] we report results for normalized median intensity, which measures color constancy of images, for the same dataset and obtained the following values: SegCN-Net - Standard Deviation(SD)= 0.011, Coefficient of Variation (CV)= 0.021, which is better than Zanjani et al. [142] - $SD = 0.0188, CV = 0.0209$.

Table 2. Segmentation results on the GLas Segmentation challenge for *SegCN – Net*, [21], [144] and the top ranked method. *HD* is in mm. Best results per metric in bold.

	<i>SegCN – Net</i>		Glas Rank 1		[21]		[144]	
	Part A	Part B	Part A	Part B	Part A	Part B	Part A	Part B
F1	0.9351	0.7542	0.912	0.716	0.926	0.728	0.922	0.729
DM	0.9212	0.8054	0.897	0.781	0.909	0.798	0.892	0.785
HD	42.276	143.286	45.418	160.347	44.243	157.643	47.012	161.321

As reported in [35], we calculate values for complex wavelet structural similarity index (CWSSIM) between real and generated images. $CWSSIM \in [0, 1]$ with higher values indicating a better match and is robust to small translations and rotations. Mean CWSSIM values of SegCN-Net is 0.82, which is higher than CycleGAN (0.75) and [35] (0.77).

4 Conclusion

We have proposed a novel approach to stain-color normalization in histopathology images, integrating semantic features into the self-supervised network. Our semantic guidance approach facilitates the inclusion of segmentation information without the need for manually segmented maps that are very difficult to obtain. Experimental results on public datasets show our approach outperforms the state of the art normalization methods when evaluated for classification and segmentation tasks. Ablation studies also show the importance of semantic guidance. Although semantic guidance is obtained from a held-out dataset, we also demonstrate that when domain-specific guidance is used, the results improve even further. This has the potential for enhancing the performance of medical image analysis tasks where annotations are not readily available.

References

1. Glas segmentation challenge results. <https://warwick.ac.uk/fac/sci/dcs/research/tia/glascontest/results/>, accessed: 2020-01-30
2. Abbet, C., Zlobec, I., Bozorgtabar, B., Thiran, J.P.: Divide-and-rule: Self-supervised learning for survival analysis in colorectal cancer. arXiv preprint arXiv:2007.03292 (2020)
3. Antony, B., Sedai, S., Mahapatra, D., Garnavi, R.: Real-time passive monitoring and assessment of pediatric eye health. In: US Patent App. US Patent App. 16/178,757 (2020)
4. Bai, W., Chen, C., Tarroni, G., Duan, J., Guitton, F., Petersen, S.E., Guo, Y., Matthews, P.M., Rueckert, D.: Self-supervised learning for cardiac mr image segmentation by anatomical position prediction. In: In Proc. MICCAI. pp. 234–241 (2019)
5. Bastide, P., Kiral-Kornek, I., Mahapatra, D., Saha, S., Vishwanath, A., Caval- lar, S.V.: Machine learned optimizing of health activity for participants during meeting times. In: US Patent App. 15/426,634 (2018)

6. Bastide, P., Kiral-Kornek, I., Mahapatra, D., Saha, S., Vishwanath, A., Cavallar, S.V.: Visual health maintenance and improvement. In: US Patent 9,993,385 (2018)
7. Bastide, P., Kiral-Kornek, I., Mahapatra, D., Saha, S., Vishwanath, A., Cavallar, S.V.: Crowdsourcing health improvements routes. In: US Patent App. 15/611,519 (2019)
8. Bejnordi, B.E., Veta, M., van Diest, P.J., van Ginneken, B., Karssemeijer, N., Litjens, G., van der Laak, J., , the CAMELYON16 Consortium: Diagnostic Assessment of Deep Learning Algorithms for Detection of Lymph Node Metastases in Women With Breast Cancer. *JAMA* **318**(22), 2199–2210 (2017)
9. BenTaieb, A., Hamarneh, G.: Adversarial stain transfer for histopathology image analysis. *IEEE Trans. Med. Imaging* **37**(3), 792–802 (2018)
10. Bozorgtabar, B., Mahapatra, D., von Teng, H., Pollinger, A., Ebner, L., Thiran, J.P., Reyes, M.: Informative sample generation using class aware generative adversarial networks for classification of chest xrays. *Computer Vision and Image Understanding* **184**, 57–65 (2019)
11. Bozorgtabar, B., Mahapatra, D., von Teng, H., Pollinger, A., Ebner, L., Thiran, J.P., Reyes, M.: Informative sample generation using class aware generative adversarial networks for classification of chest xrays. In: arXiv preprint arXiv:1904.10781 (2019)
12. Bozorgtabar, B., Mahapatra, D., Thiran, J.P.: Exprada: Adversarial domain adaptation for facial expression analysis. In *Press Pattern Recognition* **100**, 15–28 (2020)
13. Bozorgtabar, B., Rad, M.S., Mahapatra, D., Thiran, J.P.: Syndemo: Synergistic deep feature alignment for joint learning of depth and ego-motion. In: *In Proc. IEEE ICCV* (2019)
14. Bozorgtabar, B., Mahapatra, D., Thiran, J.P.: Exprada: Adversarial domain adaptation for facial expression analysis. *Pattern Recognition* **100**, 107111 (2020)
15. Bozorgtabar, B., Mahapatra, D., Zlobec, I., Rau, T.T., Thiran, J.P.: Computational pathology. *Frontiers in Medicine* **7** (2020)
16. Bozorgtabar, B., Rad, M.S., Ekenel, H.K., Thiran, J.P.: Learn to synthesize and synthesize to learn. *Computer Vision and Image Understanding* **185**, 1–11 (2019)
17. Bozorgtabar, B., Rad, M.S., Ekenel, H.K., Thiran, J.P.: Using photorealistic face synthesis and domain adaptation to improve facial expression analysis. In: *2019 14th IEEE International Conference on Automatic Face & Gesture Recognition (FG 2019)*. pp. 1–8. IEEE (2019)
18. Bozorgtabar, B., Rad, M.S., Mahapatra, D., Thiran, J.P.: Syndemo: Synergistic deep feature alignment for joint learning of depth and ego-motion. In: *Proceedings of the IEEE International Conference on Computer Vision*. pp. 4210–4219 (2019)
19. Bndi, P., , et al.: From Detection of Individual Metastases to Classification of Lymph Node Status at the Patient Level: The CAMELYON17 Challenge. *IEEE Trans. Med. Imag.* **38**(2), 550–560 (2019)
20. Clevert, D.A., Unterthiner, T., Hochreiter, S.: Fast and accurate deep network learning by exponential linear units (ELUs). In: *In Proc. ICLR* (2016)
21. Gadermayr, M., Appel, V., Klinkhammer, B.M., Boor, P., Merhof, D.: Which way round?: A study on the performance of stain-translation for segmenting arbitrarily dyed histological images. In: *MICCAI (I)*. pp. 165–173 (2018)
22. Garnavi, R., Mahapatra, D., Roy, P., Tennakoon, R.: System and method to teach and evaluate image grading performance using prior learned expert knowledge base. In: US Patent App. 10,657,838 (2020)

23. Ge, Z., Mahapatra, D., Chang, X., Chen, Z., Chi, L., Lu, H.: Improving multi-label chest x-ray disease diagnosis by exploiting disease and health labels dependencies. *Multimedia Tools and Application* **1**, 1–14 (2019)
24. Ge, Z., Mahapatra, D., Sedai, S., Garnavi, R., Chakravorty, R.: Chest x-rays classification: A multi-label and fine-grained problem. In: arXiv preprint arXiv:1807.07247 (2018)
25. Guizilini, V., Hou, R., Li, J., Ambrus, R., Gaidon, A.: Semantically-guided representation learning for self-supervised monocular depth. In: In Proc. ICLR. pp. 1–14 (2020)
26. Gupta, L., Klinkhammer, B., Boor, P., Merhof, D., Gadermayr, M.: Gan-based image enrichment in digital pathology boosts segmentation accuracy. In: MICCAI (I) . pp. 631–639 (2019)
27. He, K., Zhang, X., Ren, S., Sun, J.: Deep residual learning for image recognition. In: In Proc. CVPR (2016)
28. Janowczyk, A., Basavanthally, A., Madabhushi, A.: Stain normalization using sparse autoencoders (STANOSA): application to digital pathology. *Comput. Med. Imaging Graph* **57**, 50–61 (2017)
29. Kazemina, S., Baur, C., Kuijper, A., van Ginneken, B., Navab, N., Albarqouni, S., Mukhopadhyay, A.: Gans for medical image analysis. In: arXiv preprint arXiv:1809.06222, (2018)
30. Khan, A., Rajpoot, N., Treanor, D., Magee, D.: A nonlinear mapping approach to stain normalization in digital histopathology images using image-specific color deconvolution. *IEEE Trans. Biomed Engg.* **61**(6), 1729–1738 (2014)
31. Kingma, D.P., Ba, J.: Adam: A method for stochastic optimization. In: arXiv preprint arXiv:1412.6980, (2014)
32. Kuanar, S., Athitsos, V., Mahapatra, D., Rao, K., Akhtar, Z., Dasgupta, D.: Low dose abdominal ct image reconstruction: An unsupervised learning based approach. In: In Proc. IEEE ICIP. pp. 1351–1355 (2019)
33. Kuanar, S., Rao, K., Mahapatra, D., Bilas, M.: Night time haze and glow removal using deep dilated convolutional network. In: arXiv preprint arXiv:1902.00855 (2019)
34. Kuang, H., Guthier, B., Saini, M., Mahapatra, D., Saddik, A.E.: A real-time smart assistant for video surveillance through handheld devices. In: In Proc. ACM Intl. Conf. Multimedia. pp. 917–920 (2014)
35. Lahiani, A., Navab, N., Albarqouni, S., Klaiman, E.: Perceptual embedding consistency for seamless reconstruction of tilewise style transfer. In: In Proc. MICCAI. pp. 568–576 (2019)
36. Li, Z., Mahapatra, D., J.Tielbeek, Stoker, J., van Vliet, L., Vos, F.: Image registration based on autocorrelation of local structure. *IEEE Trans. Med. Imaging* **35**(1), 63–75 (2016)
37. Lin, T.Y., Maire, M., Belongie, S., Hays, J., Perona, P., Ramanan, D., Dollar, P., Zitnick, L.: Microsoft COCO: Common Objects in Context. In: ECCV. pp. 740–755 (2014)
38. Macenko, M., Niethammer, M., Marron, J., Borland, D., Woosley, J., Guan, X., Schmitt, C., Thomas, N.: A method for normalizing histology slides for quantitative analysis. In: Proc. In: Biomedical Imaging: From Nano to Macro, 2009. ISBI09. IEEE International Symposium on. pp. 1107–1110 (2009)
39. Mahapatra, D.: Neonatal brain mri skull stripping using graph cuts and shape priors. In: In Proc: MICCAI workshop on Image Analysis of Human Brain Development (IAHBD) (2011)

40. Mahapatra, D.: Cardiac lv and rv segmentation using mutual context information. In: Proc. MICCAI-MLMI. pp. 201–209 (2012)
41. Mahapatra, D.: Groupwise registration of dynamic cardiac perfusion images using temporal information and segmentation information. In: In Proc: SPIE Medical Imaging (2012)
42. Mahapatra, D.: Landmark detection in cardiac mri using learned local image statistics. In: Proc. MICCAI-Statistical Atlases and Computational Models of the Heart. Imaging and Modelling Challenges (STACOM). pp. 115–124 (2012)
43. Mahapatra, D.: Skull stripping of neonatal brain mri: Using prior shape information with graphcuts. *J. Digit. Imaging* **25**(6), 802–814 (2012)
44. Mahapatra, D.: Cardiac image segmentation from cine cardiac mri using graph cuts and shape priors. *J. Digit. Imaging* **26**(4), 721–730 (2013)
45. Mahapatra, D.: Cardiac mri segmentation using mutual context information from left and right ventricle. *J. Digit. Imaging* **26**(5), 898–908 (2013)
46. Mahapatra, D.: Graph cut based automatic prostate segmentation using learned semantic information. In: Proc. IEEE ISBI. pp. 1304–1307 (2013)
47. Mahapatra, D.: Joint segmentation and groupwise registration of cardiac perfusion images using temporal information. *J. Digit. Imaging* **26**(2), 173–182 (2013)
48. Mahapatra, D.: Automatic cardiac segmentation using semantic information from random forests. *J. Digit. Imaging*. **27**(6), 794–804 (2014)
49. Mahapatra, D.: Combining multiple expert annotations using semi-supervised learning and graph cuts for medical image segmentation. *Computer Vision and Image Understanding* **151**(1), 114–123 (2016)
50. Mahapatra, D.: Consensus based medical image segmentation using semi-supervised learning and graph cuts. In: arXiv preprint arXiv:1612.02166 (2017)
51. Mahapatra, D.: Semi-supervised learning and graph cuts for consensus based medical image segmentation. *Pattern Recognition* **63**(1), 700–709 (2017)
52. Mahapatra, D.: Amd severity prediction and explainability using image registration and deep embedded clustering. In: arXiv preprint arXiv:1907.03075 (2019)
53. Mahapatra, D.: Registration of histopathology images using structural information from fine grained feature maps. In: arXiv preprint arXiv:2007.02078 (2020)
54. Mahapatra, D., Agarwal, K., Khosrowabadi, R., Prasad, D.: Recent advances in statistical data and signal analysis: Application to real world diagnostics from medical and biological signals. In: *Computational and mathematical methods in medicine* (2016)
55. Mahapatra, D., Antony, B., Sedai, S., Garnavi, R.: Deformable medical image registration using generative adversarial networks. In: In Proc. IEEE ISBI. pp. 1449–1453 (2018)
56. Mahapatra, D., Bozorgtabar, B.: Retinal vasculature segmentation using local saliency maps and generative adversarial networks for image super resolution. In: arXiv preprint arXiv:1710.04783 (2017)
57. Mahapatra, D., Bozorgtabar, B.: Progressive generative adversarial networks for medical image super resolution. In: arXiv preprint arXiv:1902.02144 (2019)
58. Mahapatra, D., Bozorgtabar, B., Garnavi, R.: Image super-resolution using progressive generative adversarial networks for medical image analysis. *Computerized Medical Imaging and Graphics* **71**, 30–39 (2019)
59. Mahapatra, D., Bozorgtabar, B., Hewavitharanage, S., Garnavi, R.: Image super resolution using generative adversarial networks and local saliency maps for retinal image analysis. In: MICCAI. pp. 382–390 (2017)

60. Mahapatra, D., Bozorgtabar, B., Shao, L.: Pathological retinal region segmentation from oct images using geometric relation based augmentation. In: In Proc. IEEE CVPR. pp. 9611–9620 (2020)
61. Mahapatra, D., Bozorgtabar, B., Thiran, J.P., Shao, L.: Pathological retinal region segmentation from oct images using geometric relation based augmentation. In: arXiv preprint arXiv:2003.14119 (2020)
62. Mahapatra, D., Bozorgtabar, S., Hewavitahranage, S., Garnavi, R.: Image super resolution using generative adversarial networks and local saliencymaps for retinal image analysis. In: In Proc. MICCAI. pp. 382–390 (2017)
63. Mahapatra, D., Bozorgtabar, S., Thiran, J.P., Reyes, M.: Efficient active learning for image classification and segmentation using a sample selection and conditional generative adversarial network. In: In Proc. MICCAI (2). pp. 580–588 (2018)
64. Mahapatra, D., Buhmann, J.: Obtaining consensus annotations for retinal image segmentation using random forest and graph cuts. In: In Proc. OMIA. pp. 41–48 (2015)
65. Mahapatra, D., Buhmann, J.: Visual saliency based active learning for prostate mri segmentation. In: In Proc. MLMI. pp. 9–16 (2015)
66. Mahapatra, D., Buhmann, J.: Visual saliency based active learning for prostate mri segmentation. *SPIE Journal of Medical Imaging* **3**(1) (2016)
67. Mahapatra, D., Buhmann, J.: Automatic cardiac rv segmentation using semantic information with graph cuts. In: Proc. IEEE ISBI. pp. 1094–1097 (2013)
68. Mahapatra, D., Buhmann, J.: Analyzing training information from random forests for improved image segmentation. *IEEE Trans. Imag. Proc.* **23**(4), 1504–1512 (2014)
69. Mahapatra, D., Buhmann, J.: Prostate mri segmentation using learned semantic knowledge and graph cuts. *IEEE Trans. Biomed. Engg.* **61**(3), 756–764 (2014)
70. Mahapatra, D., Buhmann, J.: A field of experts model for optic cup and disc segmentation from retinal fundus images. In: In Proc. IEEE ISBI. pp. 218–221 (2015)
71. Mahapatra, D., Garnavi, R., Roy, P., Tennakoon, R.: System and method to teach and evaluate image grading performance using prior learned expert knowledge base. In: US Patent App. 15/459,457 (2018)
72. Mahapatra, D., Garnavi, R., Roy, P., Tennakoon, R.: System and method to teach and evaluate image grading performance using prior learned expert knowledge base. In: US Patent App. 15/814,590 (2018)
73. Mahapatra, D., Garnavi, R., Sedai, S., Roy, P.: Joint segmentation and characteristics estimation in medical images. In: US Patent App. 15/234,426 (2017)
74. Mahapatra, D., Garnavi, R., Sedai, S., Roy, P.: Retinal image quality assessment, error identification and automatic quality correction. In: US Patent 9,779,492 (2017)
75. Mahapatra, D., Garnavi, R., Sedai, S., Tennakoon, R.: Classification of severity of pathological condition using hybrid image representation. In: US Patent App. 15/426,634 (2018)
76. Mahapatra, D., Garnavi, R., Sedai, S., Tennakoon, R.: Generating an enriched knowledge base from annotated images. In: US Patent App. 15/429,735 (2018)
77. Mahapatra, D., Garnavi, R., Sedai, S., Tennakoon, R., Chakravorty, R.: Early prediction of age related macular degeneration by image reconstruction. In: US Patent App. 15/854,984 (2018)
78. Mahapatra, D., Garnavi, R., Sedai, S., Tennakoon, R., Chakravorty, R.: Early prediction of age related macular degeneration by image reconstruction. In: US Patent 9,943,225 (2018)

79. Mahapatra, D., Ge, Z.: Combining transfer learning and segmentation information with gans for training data independent image registration. In: arXiv preprint arXiv:1903.10139 (2019)
80. Mahapatra, D., Ge, Z.: Training data independent image registration with gans using transfer learning and segmentation information. In: In Proc. IEEE ISBI. pp. 709–713 (2019)
81. Mahapatra, D., Ge, Z.: Training data independent image registration using generative adversarial networks and domain adaptation. *Pattern Recognition* **100**, 1–14 (2020)
82. Mahapatra, D., Ge, Z., Sedai, S.: Joint registration and segmentation of images using deep learning. In: US Patent App. 16/001,566 (2019)
83. Mahapatra, D., Ge, Z., Sedai, S., Chakravorty, R.: Joint registration and segmentation of xray images using generative adversarial networks. In: In Proc. MICCAI-MLMI. pp. 73–80 (2018)
84. Mahapatra, D., Gilani, S., Saini, M.: Coherency based spatio-temporal saliency detection for video object segmentation. *IEEE Journal of Selected Topics in Signal Processing*. **8**(3), 454–462 (2014)
85. Mahapatra, D., J.Tielbeek, Makanyanga, J., Stoker, J., Taylor, S., Vos, F., Buhmann, J.: Automatic detection and segmentation of crohn’s disease tissues from abdominal mri. *IEEE Trans. Med. Imaging* **32**(12), 1232–1248 (2013)
86. Mahapatra, D., J.Tielbeek, Makanyanga, J., Stoker, J., Taylor, S., Vos, F., Buhmann, J.: Active learning based segmentation of crohn’s disease using principles of visual saliency. In: Proc. IEEE ISBI. pp. 226–229 (2014)
87. Mahapatra, D., J.Tielbeek, Makanyanga, J., Stoker, J., Taylor, S., Vos, F., Buhmann, J.: Combining multiple expert annotations using semi-supervised learning and graph cuts for crohn’s disease segmentation. In: In Proc: MICCAI-ABD (2014)
88. Mahapatra, D., J.Tielbeek, Vos, F., Buhmann, J.: A supervised learning approach for crohn’s disease detection using higher order image statistics and a novel shape asymmetry measure. *J. Digit. Imaging* **26**(5), 920–931 (2013)
89. Mahapatra, D., Li, Z., Vos, F., Buhmann, J.: Joint segmentation and groupwise registration of cardiac dce mri using sparse data representations. In: In Proc. IEEE ISBI. pp. 1312–1315 (2015)
90. Mahapatra, D., Routray, A., Mishra, C.: An active snake model for classification of extreme emotions. In: IEEE International Conference on Industrial Technology (ICIT). pp. 2195–2199 (2006)
91. Mahapatra, D., Roy, P., Sedai, S., Garnavi, R.: A cnn based neurobiology inspired approach for retinal image quality assessment. In: In Proc. EMBC. pp. 1304–1307 (2016)
92. Mahapatra, D., Roy, P., Sedai, S., Garnavi, R.: Retinal image quality classification using saliency maps and cnns. In: In Proc. MICCAI-MLMI. pp. 172–179 (2016)
93. Mahapatra, D., Roy, S., Sun, Y.: Retrieval of mr kidney images by incorporating spatial information in histogram of low level features. In: In 13th International Conference on Biomedical Engineering (2008)
94. Mahapatra, D., Saha, S., Vishwanath, A., Bastide, P.: Generating hyperspectral image database by machine learning and mapping of color images to hyperspectral domain. In: US Patent App. 15/949,528 (2019)
95. Mahapatra, D., Saini, M., Sun, Y.: Illumination invariant tracking in office environments using neurobiology-saliency based particle filter. In: IEEE ICME. pp. 953–956 (2008)

96. Mahapatra, D., Schüffler, P., Tielbeek, J., Vos, F., Buhmann, J.: Semi-supervised and active learning for automatic segmentation of crohn's disease. In: Proc. MICCAI, Part 2. pp. 214–221 (2013)
97. Mahapatra, D., Sedai, S., Garnavi, R.: Elastic registration of medical images with gans. In: arXiv preprint arXiv:1805.02369 (2018)
98. Mahapatra, D., Sun, Y.: Nonrigid registration of dynamic renal MR images using a saliency based MRF model. In: Proc. MICCAI. pp. 771–779 (2008)
99. Mahapatra, D., Sun, Y.: Registration of dynamic renal mr images using neurobiological model of saliency. In: Proc. ISBI. pp. 1119–1122 (2008)
100. Mahapatra, D., Sun, Y.: Using saliency features for graphcut segmentation of perfusion kidney images. In: In 13th International Conference on Biomedical Engineering (2008)
101. Mahapatra, D., Sun, Y.: Joint registration and segmentation of dynamic cardiac perfusion images using mrfs. In: Proc. MICCAI. pp. 493–501 (2010)
102. Mahapatra, D., Sun, Y.: An mrf framework for joint registration and segmentation of natural and perfusion images. In: Proc. IEEE ICIP. pp. 1709–1712 (2010)
103. Mahapatra, D., Sun, Y.: Retrieval of perfusion images using cosegmentation and shape context information. In: Proc. APSIPA Annual Summit and Conference (ASC) (2010)
104. Mahapatra, D., Sun, Y.: Rigid registration of renal perfusion images using a neurobiology based visual saliency model. EURASIP Journal on Image and Video Processing. pp. 1–16 (2010)
105. Mahapatra, D., Sun, Y.: A saliency based mrf method for the joint registration and segmentation of dynamic renal mr images. In: Proc. ICDIP (2010)
106. Mahapatra, D., Sun, Y.: Mrf based intensity invariant elastic registration of cardiac perfusion images using saliency information. IEEE Trans. Biomed. Engg. **58**(4), 991–1000 (2011)
107. Mahapatra, D., Sun, Y.: Orientation histograms as shape priors for left ventricle segmentation using graph cuts. In: In Proc: MICCAI. pp. 420–427 (2011)
108. Mahapatra, D., Sun, Y.: Integrating segmentation information for improved mrf-based elastic image registration. IEEE Trans. Imag. Proc. **21**(1), 170–183 (2012)
109. Mahapatra, D., Tielbeek, J., Buhmann, J., Vos, F.: A supervised learning based approach to detect crohn's disease in abdominal mr volumes. In: Proc. MICCAI workshop Computational and Clinical Applications in Abdominal Imaging(MICCAI-ABD). pp. 97–106 (2012)
110. Mahapatra, D., Tielbeek, J., Vos, F., ., J.B.: Crohn's disease tissue segmentation from abdominal mri using semantic information and graph cuts. In: Proc. IEEE ISBI. pp. 358–361 (2013)
111. Mahapatra, D., Tielbeek, J., Vos, F., Buhmann, J.: Localizing and segmenting crohn's disease affected regions in abdominal mri using novel context features. In: Proc. SPIE Medical Imaging (2013)
112. Mahapatra, D., Tielbeek, J., Vos, F., Buhmann, J.: Weakly supervised semantic segmentation of crohn's disease tissues from abdominal mri. In: Proc. IEEE ISBI. pp. 832–835 (2013)
113. Mahapatra, D., Vos, F., Buhmann, J.: Crohn's disease segmentation from mri using learned image priors. In: In Proc. IEEE ISBI. pp. 625–628 (2015)
114. Mahapatra, D., Vos, F., Buhmann, J.: Active learning based segmentation of crohns disease from abdominal mri. Computer Methods and Programs in Biomedicine **128**(1), 75–85 (2016)
115. Mahapatra, D., Winkler, S., Yen, S.: Motion saliency outweighs other low-level features while watching videos. In: SPIE HVEI. pp. 1–10 (2008)

116. Mahapatra, D., Bozorgtabar, B.: Retinal vasculature segmentation using local saliency maps and generative adversarial networks for image super resolution. arXiv preprint arXiv:1710.04783 (2017)
117. Mahapatra, D., Bozorgtabar, B.: Progressive generative adversarial networks for medical image super resolution. arXiv preprint arXiv:1902.02144 (2019)
118. Rad, M.S., Yu, T., Musat, C., Ekenel, H.K., Bozorgtabar, B., Thiran, J.P.: Benefitting from bicubically down-sampled images for learning real-world image super-resolution. arXiv preprint arXiv:2007.03053 (2020)
119. Reinhard, E., Adhikhmin, M., Gooch, B., Shirley, P.: Color transfer between images. *IEEE Comput. Graphics Appl.* **21**(5), 34–41 (2001)
120. Ronneberger, O., Fischer, P., Brox, T.: U-net: Convolutional networks for biomedical image segmentation. In: *In Proc. MICCAI*. pp. 234–241 (2015)
121. Ross, T., et al.: Gexploiting the potential of unlabeled endoscopic video data with self-supervised learning. *International Journal of Computer Assisted Radiology and Surgery* volume **13**, 925–933 (2018)
122. Roy, P., Chakravorty, R., Sedai, S., Mahapatra, D., Garnavi, R.: Automatic eye type detection in retinal fundus image using fusion of transfer learning and anatomical features. In: *In Proc. DICTA*. pp. 1–7 (2016)
123. Roy, P., Tennakoon, R., Cao, K., Sedai, S., Mahapatra, D., Maetschke, S., Garnavi, R.: A novel hybrid approach for severity assessment of diabetic retinopathy in colour fundus images. In: *In Proc. IEEE ISBI*. pp. 1078–1082 (2017)
124. Saini, M., Guthier, B., Kuang, H., Mahapatra, D., Saddik, A.: szoom: A framework for automatic zoom into high resolution surveillance videos. In: arXiv preprint arXiv:1909.10164 (2019)
125. Schüffler, P., Mahapatra, D., Tielbeek, J., Vos, F., Makanyanga, J., Pends, D., Nio, C., Stoker, J., Taylor, S., Buhmann, J.: A model development pipeline for crohns disease severity assessment from magnetic resonance images. In: *In Proc: MICCAI-ABD* (2013)
126. Schüffler, P., Mahapatra, D., Tielbeek, J., Vos, F., Makanyanga, J., Pends, D., Nio, C., Stoker, J., Taylor, S., Buhmann, J.: Semi automatic crohns disease severity assessment on mr imaging. In: *In Proc: MICCAI-ABD* (2014)
127. Sedai, S., Mahapatra, D., Antony, B., Garnavi, R.: Joint segmentation and uncertainty visualization of retinal layers in optical coherence tomography images using bayesian deep learning. In: *In Proc. MICCAI-OMIA*. pp. 219–227 (2018)
128. Sedai, S., Mahapatra, D., Ge, Z., Chakravorty, R., Garnavi, R.: Deep multiscale convolutional feature learning for weakly supervised localization of chest pathologies in x-ray images. In: *In Proc. MICCAI-MLMI*. pp. 267–275 (2018)
129. Sedai, S., Mahapatra, D., Hewavitharanage, S., Maetschke, S., Garnavi, R.: Semi-supervised segmentation of optic cup in retinal fundus images using variational autoencoder. In: *In Proc. MICCAI*. pp. 75–82 (2017)
130. Sedai, S., Roy, P., Mahapatra, D., Garnavi, R.: Segmentation of optic disc and optic cup in retinal fundus images using shape regression. In: *In Proc. EMBC*. pp. 3260–3264 (2016)
131. Sedai, S., Roy, P., Mahapatra, D., Garnavi, R.: Segmentation of optic disc and optic cup in retinal images using coupled shape regression. In: *In Proc. MICCAI-OMIA*. pp. 1–8 (2016)
132. Shaban, M.T., Baur, C., Navab, N., Albarqouni, S.: StainGAN: Stain style transfer for digital histological images. arXiv preprint arXiv:1804.01601 (2018)
133. Sirinukunwattana, K., et al.: Gland segmentation in colon histology images: The GlaS challenge contest. *Med. Imag. Anal.* **35**, 489–502 (2017)

134. Su, H., Jampani, V., Sun, D., Gallo, O., Learned-Miller, E., Kautz, J.: Pixel-adaptive convolutional neural networks. In: In Proc. IEEE CVPR. pp. 11166–11175 (2019)
135. Tajbakhsh, N., Hu, Y., Cao, J., Yan, X., Xiao, Y., Lu, Y., Liang, J., Terzopoulos, D., Ding, X.: Surrogate supervision for medical image analysis: Effective deep learning from limited quantities of labeled data. In: In Proc. IEEE ISBI. pp. 1251–1255 (2019)
136. Tennakoon, R., Mahapatra, D., Roy, P., Sedai, S., Garnavi, R.: Image quality classification for dr screening using convolutional neural networks. In: In Proc. MICCAI-OMIA. pp. 113–120 (2016)
137. Vahadane, A., Peng, T., Sethi, A., Albarqouni, S., Wang, L., Baust, M., Steiger, K., Schlitter, A.M., Esposito, I., Navab., N.: Structure-preserving color normalization and sparse stain separation for histological images. *IEEE IEEE Trans. Med. Imag.* **35**(8), 1962–1971 (2016)
138. Vos, F.M., Tielbeek, J., Naziroglu, R., Li, Z., Schüffler, P., Mahapatra, D., Wiebel, A., Lavini, C., Buhmann, J., Hege, H., Stoker, J., van Vliet, L.: Computational modeling for assessment of IBD: to be or not to be? In: Proc. IEEE EMBC. pp. 3974–3977 (2012)
139. Wu, Y., He, K.: Group normalization. In: In Proc. ECCV. pp. 3–19 (2018)
140. Xing, Y., Ge, Z., Zeng, R., Mahapatra, D., Seah, J., Law, M., Drummond, T.: Adversarial pulmonary pathology translation for pairwise chest x-ray data augmentation. In: In Proc. MICCAI. pp. 757–765 (2019)
141. Yi, X., Walia, E., Babyn, P.: Generative adversarial network in medical imaging: A review. *Med. Imag. Anal.* **58** (2019)
142. Zanjani, F.G., Zinger, S., Bejnordi, B.E., van der Laak, J.A.: Histopathology stain-color normalization using deep generative models. In: Proc. Medical Imaging with Deep Learning (2018)
143. Zhao, M., Wang, L., et al.: Craniomaxillofacial bony structures segmentation from mri with deep-supervision adversarial learning. In: MICCAI. pp. 720–727 (2018)
144. Zhou, N., Cai, D., Han, X., Yao, J.: Enhanced cycle-consistent generative adversarial network for color normalization of h&e stained images. In: MICCAI (I). pp. 694–702 (2019)
145. Zhu, J., T.park, Isola, P., Efros, A.: Unpaired image-to-image translation using cycle-consistent adversarial networks. In: arXiv preprint arXiv:1703.10593 (2017)
146. Zilly, J., Buhmann, J., Mahapatra, D.: Boosting convolutional filters with entropy sampling for optic cup and disc image segmentation from fundus images. In: In Proc. MLMI. pp. 136–143 (2015)
147. Zilly, J., Buhmann, J., Mahapatra, D.: Glaucoma detection using entropy sampling and ensemble learning for automatic optic cup and disc segmentation. In Press *Computerized Medical Imaging and Graphics* **55**(1), 28–41 (2017)